



Efficient recovery of bisphenol A from aqueous solution using K_2CO_3 activated carbon derived from starch-based polyurethane

Ke Wang¹ · Xingzhen Qin¹ · Kungang Chai¹ · Zongwu Wei² · Fan Deng¹ · Bingyu Liao³ · Jinyu Wu¹ · Fang Shen¹ · Zhi Zhang³

Received: 6 January 2023 / Accepted: 24 April 2023 / Published online: 28 April 2023
© The Author(s), under exclusive licence to Springer-Verlag GmbH Germany, part of Springer Nature 2023

Abstract

Endocrine-disrupting compounds (EDCs) are increasingly polluting water, making it of practical value to develop novel desirable adsorbents for removing these pollutants from wastewater. Here, a simple cross-linking strategy combined with gentle chemical activation was demonstrated to prepare starch polyurethane-activated carbon (STPU-AC) for adsorbing BPA in water. The adsorbents were characterized by various techniques such as FTIR, XPS, Raman, BET, SEM, and zeta potential, and their adsorption properties were investigated comprehensively. Results show that STPU-AC possesses a large surface area ($1862.55 \text{ m}^2 \cdot \text{g}^{-1}$) and an abundance of functional groups, which exhibited superior adsorption capacity for BPA ($543.4 \text{ mg} \cdot \text{g}^{-1}$) and favorable regenerative abilities. The adsorption of BPA by STPU-AC follows a pseudo-second-order kinetic model and a Freundlich isotherm model. The effect of aqueous solution chemistry (pH and ionic strength) and the presence of other contaminants (phenol, heavy metals, and dyes) on BPA adsorption was also analyzed. Moreover, theoretical studies further demonstrate that hydroxyl oxygen and pyrrole nitrogen are the primary adsorption sites. We found that the efficient recovery of BPA was associated with pore filling, hydrogen-bonding interaction, hydrophobic effects, and π - π stacking. These findings demonstrate the promising practical application of STPU-AC and provide a basis for the rational design of starch-derived porous carbon.

Keywords Adsorption · Bisphenol A · Porous carbon · Starch · Theoretical calculation · Simulated effluents

Introduction

Bisphenol A (BPA), a typical endocrine disruptor (EDC) (Martinez et al. 2020), has been widely used in the manufacture of polymeric materials (including polyphenylene ether resins and epoxy resins) as well as fine chemicals like plasticizers (Zhang et al. 2022b; Lee et al. 2021;

Shao et al. 2021). Massive BPA emissions have been linked to several underlying health problems, including metabolic disorders and cancer (M'Rabet et al. 2019; Karthikeyan et al. 2019). Furthermore, BPA and phenol inevitably co-exist in the related industrial wastewater during the production of BPA by the condensation of acetone and phenol, posing a significant environmental hazard. Therefore, the recovery of BPA from aqueous solutions was of particular interest. Researchers have investigated membrane separation (Zhao et al. 2021; Yang et al. 2021; Rana et al. 2014; Chen et al. 2020), photocatalytic degradation (Wang et al. 2021b; Kim et al. 2022; Han et al. 2021), and adsorption (Mpatani et al. 2020; Lv et al. 2021; Jiang et al. 2021) to remove BPA from aqueous solutions. Due to its simplicity, efficiency, and eco-friendliness, adsorption is considered a highly effective contaminant removal method, and adsorbents usually dominate in adsorption process (Heo et al. 2019; Bhatnagar and Anastopoulos 2017). Various adsorbents could remove EDCs from aqueous environments, such

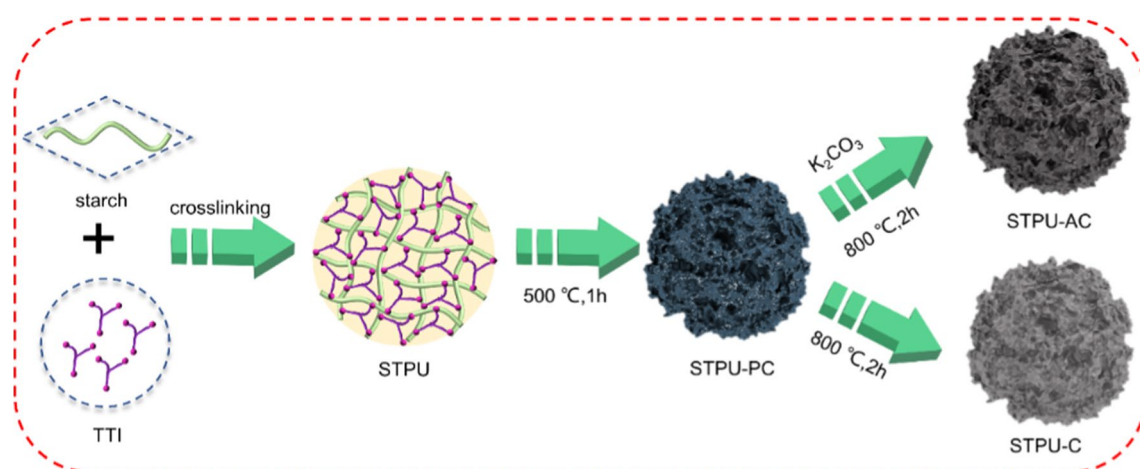
Responsible Editor: Tito Roberto Cadaval Jr

✉ Fang Shen
fangshen@gxu.edu.cn

¹ School of Chemistry and Chemical Engineering, Guangxi Key Laboratory of Petrochemical Resource Processing and Process Intensification Technology, Guangxi University, Nanning 530004, Guangxi, China

² School of Resources, Environment and Materials, Guangxi University, Nanning 530004, Guangxi, China

³ Guangxi Xiangsheng Household Materials Technology Co., Ltd., Chongzuo 532200, Guangxi, China



Scheme 1 Synthesis procedure of starch-based carbon samples

as porous resins (Xu et al. 2019; Yuan et al. 2022), metal–organic–frameworks (Khan et al. 2013; Han et al. 2022), silica (Xiao et al. 2015; Pellicer-Castell et al. 2022; Kittappa et al. 2020), and porous carbon (Zhang et al. 2018; Wang et al. 2022; Qu et al. 2022; Mpatani et al. 2021; Cheng et al. 2019).

Among various adsorbents, carbon materials have become ideal materials for treating phenol-containing wastewater due to their large specific surface area (Javed et al. 2018), rich pore structure, and ultra-high chemical stability. For example, Wang et al. (Wang et al. 2022) constructed graded porous carbon nanosheets (ZG-C) with high adsorption capacity (602.2 mg g^{-1}) for BPA, demonstrating that topological defects play an integral role in facilitating adsorption. Previously, Pan et al. investigated the adsorption of BPA on carbon nanomaterials, showing very good potential for removing BPA from water (Pan et al. 2008). However, most activated carbons have few functional groups and interaction sites on the surface, resulting in insufficient adsorption capacity. Activated carbon surface modification technology has been found to be an effective method to improve their performance. In a study by Alves et al., the authors found that by modifying the functional groups on the surface of activated carbon, it was possible to modulate its surface chemistry to enhance the adsorption capacity for pollutants (Alves et al. 2021). Meanwhile, heteroatoms (N, S, et al.) can provide more adsorption sites on the surface of activated carbon, contributing to improving the material properties (Wang et al. 2021a; Ahamad et al. 2019; Cui et al. 2019). For example, Heo et al. found a novel magnetic biochar substance (CZF-biochar) to adsorb both BPA and sulfamethoxazole

simultaneously (Heo et al. 2019). Researchers (Qu et al. 2022) successfully prepared magnetic nitro-doped porous biochar (Fe/N-PBC) with good adsorption properties for Cr (VI) and BPA. Therefore, the rational use of modifications was essential to improve the adsorption efficiency of carbon materials.

Considering the cost and reserves of starch, its advantages of biodegradability and ease of modification (Yuan et al. 2022) could be a potential natural substrate for preparing biomass sorbents (Cazotti et al. 2020). Meanwhile, triphenylmethane -4,4',4''-trisisocyanate (TTI), a common organic raw material with low cost (the price of TTI was 300 CNY per kilogram), allows polymeric materials to be linked together in web-shaped structures containing oxygen and nitrogen (Zhao et al. 2022; Ghafari et al. 2019). In recent years, it has been discovered that carbon-based materials prepared using starch effectively remove contaminants (Yao et al. 2022; Zhang et al. 2022a). However, the recovery of BPA from activated carbon derived from starch-crosslinked polyurethane materials has yet to be reported.

Therefore, we have developed a starch polyurethane-activated carbon material (STPU-AC) with a high specific surface area by selecting a green starch cross-linked polyurethane as a carbon precursor combined with milder potassium carbonate as an activator. The process for synthesizing is displayed in Scheme 1. The adsorbent has been characterized by various techniques including FTIR, XPS, Raman, BET, and SEM. Based on adsorption experiments and theoretical calculations, we explored the adsorption mechanism of the developed activated carbon and evaluated its regeneration capacity. The results showed that STPU-AC is a practical and environmentally friendly material for treating wastewater containing BPA.

Materials and methods

Materials

Triphenylmethane -4,4',4''-triisocyanate (TTI, ethyl acetate solution, w/w = 27%) was provided by Hubei Xinmingtai Chemistry Co., Ltd. Soluble starch, BPA, methylene blue (MB), copper nitrate ($\text{Cu}(\text{NO}_3)_2$), and phenol were acquired by Shanghai Aladdin Biochemical Technology Co. Sodium diethyldithiocarbamate was bought from Shanghai Macklin Biochemical Technology Co., Ltd. Anhydrous N, N-dimethylformamide (DMF, AR) was ordered at Shanghai Titan Scientific Co., Ltd. Analytical grade acetone, methanol, ethanol, and ethyl acetate, from Kelong Chemical Reagent Factory, Chengdu. Anhydrous K_2CO_3 (AR) was procured from Beijing Macklin Biochemical Company. The solution in experiments was prepared with ultrapure water.

Preparation of STPU-AC

The starch-based polyurethane (STPU) was prepared by catalyst-free one-step polymerization. Typically, soluble starch (0.5 g) was dissolved in 20 mL of DMF at 70 °C, followed by the addition of TTI solution (1.5 mmol, 2.039 g). The reaction was conducted at 70 °C for 4 h with constant stirring. The polymer products were washed copiously with acetone and dried to stable weight to obtain a purple polymer product.

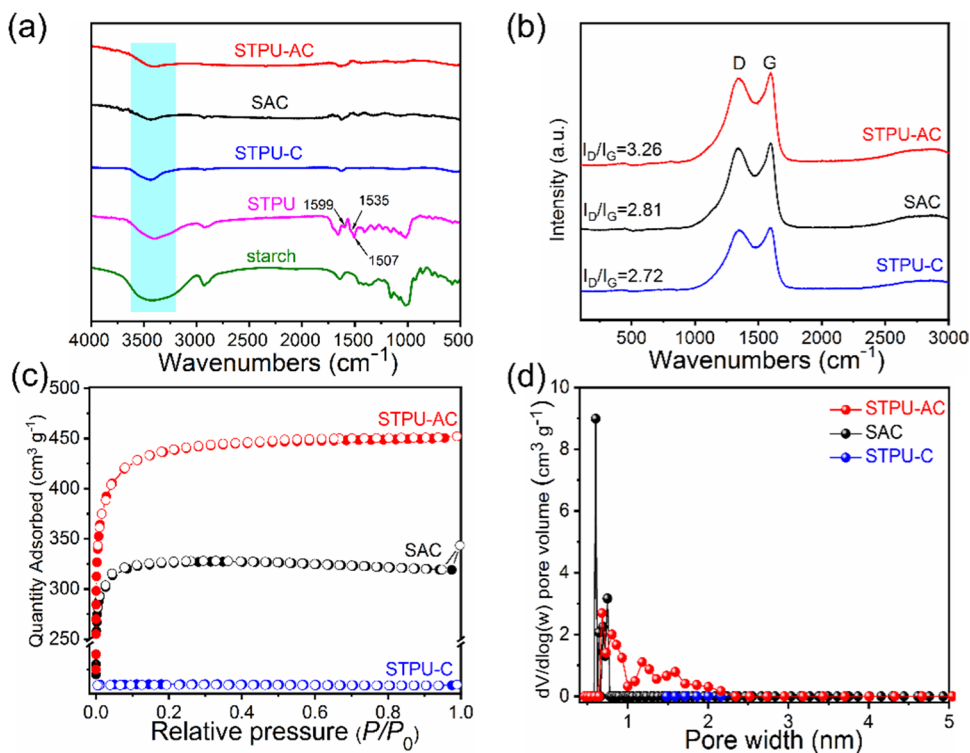
Second, the carbon materials were synthesized through chemical activation with K_2CO_3 . Briefly, the polymer was

pre-carbonized at 500 °C for 1 h under an N_2 atmosphere, blended with K_2CO_3 at ratio of 1:2 and heated to 800 °C for 2 h. Lastly, the products were washed with deionized water and then oven-dried at 60 °C for 12 h, marked as STPU-AC. As a comparison, the starch polyurethane carbon-based material (STPU-C) was fabricated with the same process except without K_2CO_3 modification. The starch-derived activated carbon (SAC) was prepared by hydrothermal carbonization and chemical activation with K_2CO_3 . Supplementary information (Text S1) gave details of the preparation of the SAC.

Characterization

Fourier transform infrared (FTIR) spectra with wavelengths of 4000–400 cm^{-1} were acquired on the TENSOR II spectrometer (Bruker). Raman spectra were recorded on a Raman spectrometer (Thermo Fisher DXR) with a 532 nm laser. The structure of the samples was measured by X-ray diffraction (XRD, Smartlab-3kw diffractometer, Japan). The N_2 adsorption/desorption isotherms were measured with an ASAP 2460 instrument (Micromeritics). X-ray photoelectron spectroscopy (XPS) was used to analyze the surface chemical state of products with a K-Alpha spectrometer (Thermo Scientific). Elemental analyzer (Vario Micro Cube, German) was used to determine the content of C, H, and O. The scanning electron microscope (SEM, Hitachi) was used to record the surface morphology of materials. The DFT calculations were done at the high-performance computing platform of Guangxi University.

Fig. 1 a FT-IR spectra, b Raman spectra, c N_2 adsorption/desorption isotherms, and d pore size distribution



Adsorption experiments

In single-component experiments, 10 mg of STPU-C, SAC, and STPU-AC was mixed with 20 mL of different concentrations (50, 150, and 300 mg L⁻¹) of BPA solution and shaken for 12 h at 25 °C to reach adsorption equilibrium. After filtration through a membrane (0.22 μm, PTFE), the BPA concentrations were measured with a UV–visible spectrophotometer (UV-2600).

We prepared six groups of multi-component solutions for the two-component adsorption experiments. The BPA concentration was kept constant at 300 mg•L⁻¹, and the phenol concentrations were divided at 0, 60, 120, 180, 240, and 300 mg•L⁻¹. Each component concentration was determined by high-performance liquid chromatography (HPLC). In the experiments with ternary pollutants (mixture concentration of 100 mg•L⁻¹), the concentration of each component was analyzed by UV–visible spectrophotometry.

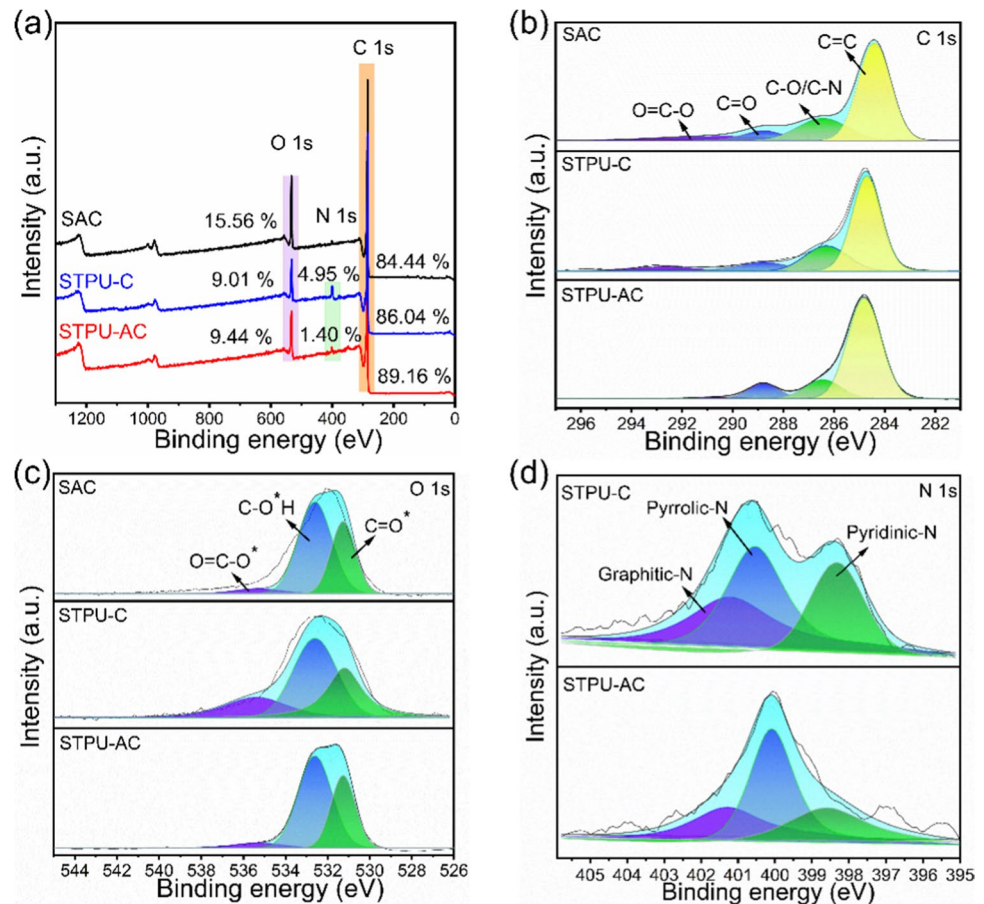
Adsorption experiments were performed to investigate the kinetics. Specifically, 125 mg of the adsorbent was placed in 250 mL of BPA (300 mol•L⁻¹) solution under magnetic stirring at 25 °C, taking samples at predetermined time intervals until it reached equilibrium. The adsorption capacity at different temperatures (298.15, 308.15, and 318.15 K) was

studied to obtain the adsorption isotherm. Kinetic and isotherm correlation models (Text S2) analyze the adsorption process.

To investigate the effect of pH value and ionic strength on adsorption, 0.2 mol•L⁻¹ HCl and NaOH solutions were prepared to adjust BPA (300 mol•L⁻¹) with different pH value solutions. Moreover, various amounts of NaCl were added into the BPA (300 mol•L⁻¹) solution to prepare the ionic strength of the solution (0.1, 0.2, 0.3, 0.4, and 0.5 mol•L⁻¹), respectively.

The reusability of STPU-AC was investigated. First, 10 mg of BPA-loaded STPU-AC was dissolved in 10 mL of different polar eluents (ethyl acetate, acetone, ethanol, and methanol), and the concentration of BPA in the eluent was analyzed by high-performance liquid chromatography to explore the best eluent (ethanol). Afterwards, the BPA-loaded STPU-AC was immersed in ethanol and dried following shaking at 25 °C for 4 h to obtain the recovered STPU-AC for a new adsorption cycle under the same adsorption conditions, and this process was repeated 10 times. While all adsorption experiments were performed three times, the supplementary information (Text S2 and Fig S5) provides further detail for each adsorption experiment.

Fig. 2 a XPS survey spectra, high resolution spectra of **b** C 1s, **c** O 1s, and **d** N 1s for carbon samples



The adsorption capacity q_e (mg g^{-1}) and the recovery efficiency AR (%) were calculated by the following formula:

$$q_e = \frac{(C_0 - C_e)V}{m} \quad (1)$$

$$\text{AR}(\%) = \frac{C_0 - C_e}{C_0} \times 100\% \quad (2)$$

in which V (L) and m (g) are the volumes of the solution and the mass of adsorbent, respectively; C_0 and C_e ($\text{mg}\cdot\text{L}^{-1}$) are the initial concentration and the equilibrium concentrations, respectively.

Theoretical calculation

Based on density functional theory (DFT), all theoretical calculations were carried out at the M062X/6-31G (Ruiz 2008) level by GAUSSIAN 16 software. First, the structures of the adsorbed substrates and adsorbents were optimized, see Fig. S1. Independent gradient models (IGMs) (Lu and Chen 2012) were used to investigate the weak interactions during adsorption and visualized using VMD

1.9.3 software (Humphrey et al. 1996). E_{ads} (kJ mol^{-1}) (Wei et al. 2019) was calculated with the following formula:

$$E_{\text{ads}} = E_{\text{sys}} - (E_{\text{ad}} + E_{\text{sub}}) \quad (3)$$

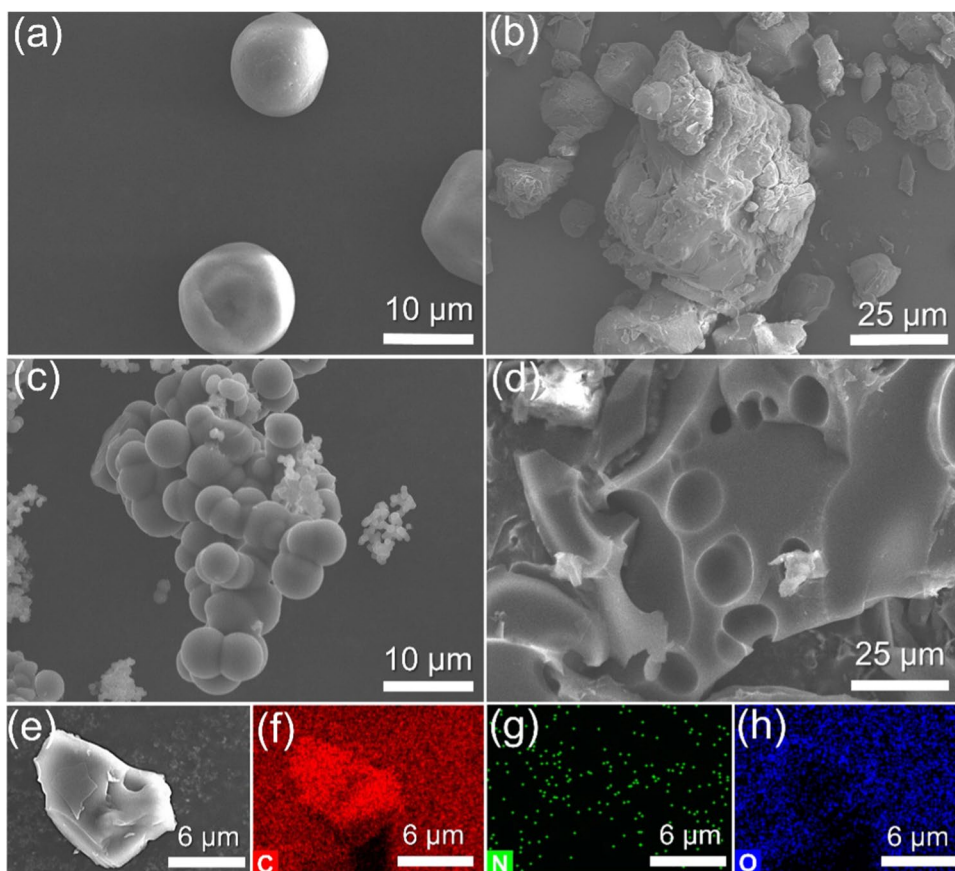
where E_{sys} , E_{ad} , and E_{sub} stand for the energies of systems, adsorbent, and substrate, respectively.

Results and discussion

Characterization of related carbons

To determine its surface functional groups, we conducted FT-IR analysis on the adsorbent. Illustrated in Fig. 1a, STPU appeared in new bands at 1535 cm^{-1} , 1507 , and 1599 cm^{-1} , which were connected to the skeletal vibrations of N–H and benzene rings, respectively, indicating the successful introduction of polyurethane units (Zhou et al. 2020). However, most organic groups disappeared after pyrolysis, exhibiting similar FT-IR spectra, illustrating that the starch-derived biochar has a similar structural and functional group. Notably, after K_2CO_3 modification, the O–H (3340 cm^{-1}) vibrational peak of STPU-AC and SAC was moderately weakened,

Fig. 3 SEM images of (a) starch, (b) STPU, (c) SAC, (d) STPU-AC, and (e–h) EDS elemental mapping images of STPU-AC



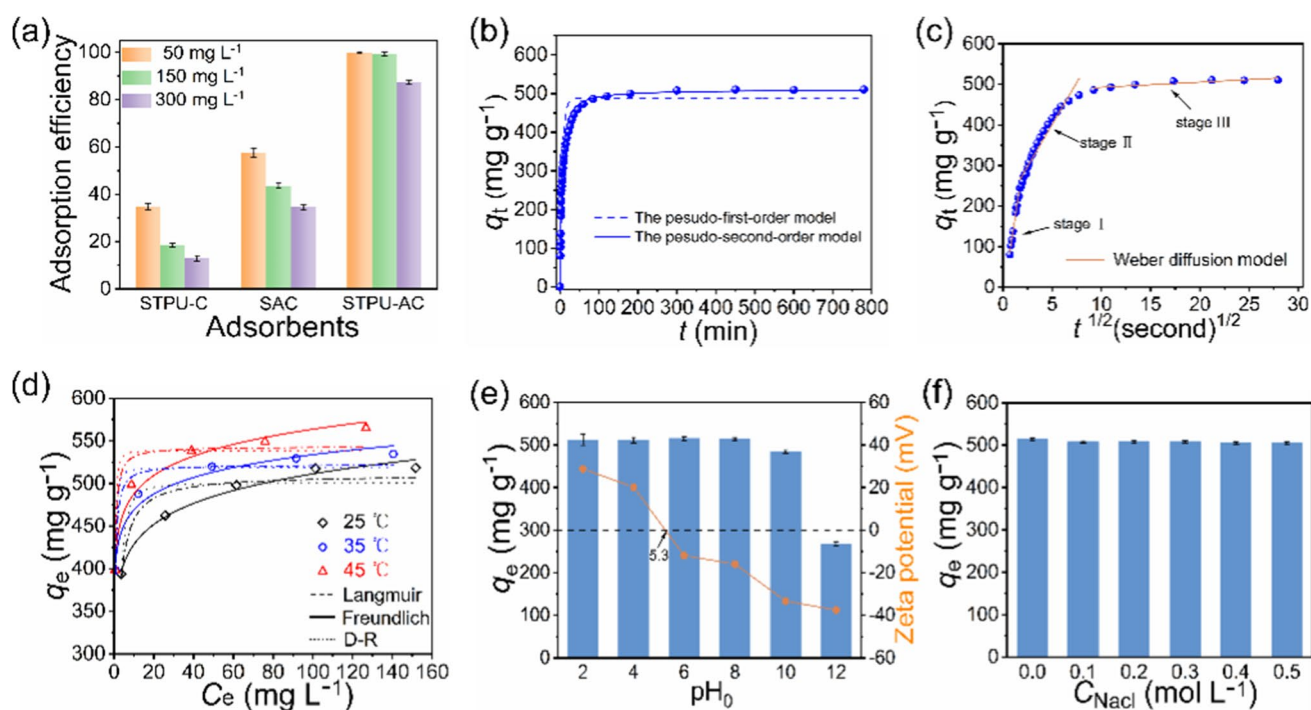


Fig. 4 (a) Adsorption efficiency of BPA by different carbonaceous adsorbents with various initial concentrations, adsorbent dosage (10 mg) and volume of solution (20 mL), (b, c) adsorption kinetics of BPA onto STPU-AC with the non-linear fittings, (d) adsorption

isotherms of BPA onto STPU-AC at 25, 35 and 45 °C, the effects of (e) initial pH, and (f) ionic strength on the adsorption of BPA onto STPU-AC

which could be interpreted by further oxygen consumption during pyrolytic activation.

Furthermore, as demonstrated in Fig. 1b, Raman spectroscopy confirmed the defective nature of porous carbon. The sample exhibits two typical broad peaks at 1363 cm^{-1} (D band) and 1589 cm^{-1} (G band). Typically, the G peak indicates the E_{2g} symmetry, related to the vibration of sp^2 hybridized carbon atoms in the graphitic layer. The D peak denotes the defect degree of the graphitic structure. Furthermore, the I_D/I_G values of STPU-AC increased significantly, indicating that the activation process generated more defects in biochar, consistent with the experimental results obtained from Xiao et al. (Xiao et al. 2018). Additionally, according to the XRD pattern (see Fig. S4), the diffraction peaks of the carbon material were diminished, indicating that the carbon was highly disordered in our sample.

N_2 adsorption–desorption studies were performed to explore the porous structure of the material. Figure 1c and d demonstrate the N_2 adsorption–desorption isotherms and pore size distributions of the carbon materials. Based on the same carbon source, STPU-AC exhibited a significantly higher nitrogen adsorption capacity than STPU-C, indicating that the material formed after activation facilitates the creation of additional pores. These additional pores and the realization that SAC has marginally lower nitrogen adsorption

than STPU-AC imply that the carbon source is crucial. Furthermore, SAC and STPU-AC have type I adsorption curves, indicating that the materials are primarily composed of micropores, like previous findings. As depicted in Fig. 1d, STPU-AC has a wider pore structure distribution than SAC in the micropore distribution range, which makes it more suitable for pollutant adsorption. Based on the detailed parameters in Table S1, STPU-AC has a greater specific surface area and maximum pore volume, which providing an excellent structural foundation for its fast adsorption of pollutants in water.

XPS tests were performed to evaluate the material's surface composition and chemical state, as displayed in Fig. 2a. The XPS survey spectrum has distinct peaks for C1s, N1s, and O1s, indicating the presence of C, N, and O on the sample surface. During activation, the nitrogen content dropped from 4.95% to 1.4%, meaning that some nitrogen-containing functional groups were consumed during the pyrolysis. Based on the high-resolution spectra of C1s (Fig. 2b), peaks with binding energies of 284.8, 286.3, 288.8, and 289.6 eV were assigned to the C=C, C–O/C–N, C=O, and O=C–O functional groups, respectively. sp^2 -C atoms on the surface of STPU-AC exhibited high electron density. The aromatic ring of the BPA molecule interacts with the STPU-AC surface via π - π interactions. The spectrum of the O1s region is presented in Fig. 2c, with three

distinct peaks at 531.2, 532.3, and 535.4 eV corresponding to the C=O*, C–O*H, and O*–C=O functional groups, respectively. Figure 2d depicts the N1s XPS spectra of STPU-AC and STPU-C, with peaks at 401, 400.1, and 398.6 eV ascribed to graphite N, pyrrole N, and pyridine N species, respectively, and the results revealed that pyrrole N is the predominant form of N atom in STPU-AC. Meanwhile, Table S2–S4 summarize the detailed contents of the samples' functional groups of C1s, O1s, and N1s. The agreement between the XPS and elemental analysis (Table S5) results further confirms the presence of oxygen- and nitrogen-containing functional groups on the surface of STPU-AC. These functional groups play a crucial role in forming active sites on the carbon material.

The surface morphological properties of the material were recorded by SEM, as illustrated in Fig. 3. The pure starch appeared smooth and spherical, and the SAC agglomerated together and retained a spherical shape after pyrolysis and chemical activation (Fig. 3a and c). After crosslinking, the surface of the STPU turned rough and agglomerated (Fig. 3b). In addition, the morphology of STPU-AC changed dramatically with holes formed in the surface due to the chemical etching (Fig. 3d). Furthermore, the EDS elemental mapping in Fig. 3e–h demonstrates that the elements C, N, and O are dispersed uniformly across the surface of STPU-AC.

BPA recovery tests in water

Screening of optimal adsorbent for BPA adsorption

Comparative experiments were conducted on samples under the same conditions to determine the effect of initial adsorbent concentration on BPA removal efficiency. As demonstrated in Fig. 4a, the removal efficiency of all three materials decreased with the increasing initial concentration of BPA. The removal of BPA from the samples was followed by STPU-AC > SAC > STPU-C for the same adsorbent concentration, demonstrating that pore structure is mainly responsible for BPA adsorption. Meanwhile, this phenomenon confirmed the significance of porous activation of biochar for removing BPA. In other words, the synergistic effect of the micropores and functional groups resulted in STPU-AC showing the highest adsorption capacity.

Table 1 Thermodynamic parameters of BPA adsorption onto STPU-AC

Temperature (°C)	ΔG^0 (kJ mol ⁻¹)	ΔH^0 (kJ mol ⁻¹)	ΔS^0 (J mol ⁻¹ K ⁻¹)
25	-26.71		
35	-31.48	65.29	310.36
45	-32.84		

Accordingly, subsequent experiments have used this material as an adsorbent.

Adsorption kinetic analysis

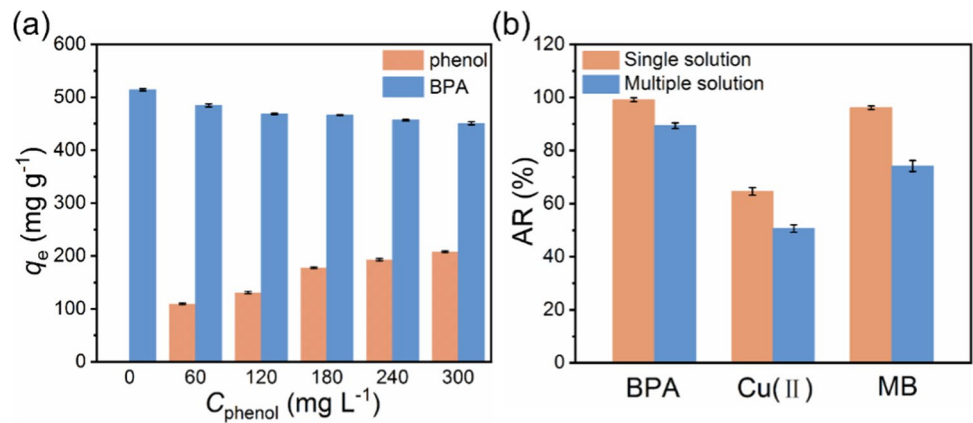
The effect of contact time on BPA adsorption by STPU-AC was investigated. As depicted in Fig. 4b, the adsorption amount increased dramatically within the first 30 min, reaching 86.5% of the equilibrium point for BPA uptake. This trend can be explained by the microporous structure of STPU-AC, which provides more adsorption sites for BPA adsorption and accelerates molecular mass transfer (Ahmad et al. 2019). However, with increasing contact time, more adsorption sites were occupied, and the BPA adsorption process slowed down and attained equilibrium within 2 h.

Several kinetic models, such as pseudo-first-order and pseudo-second-order, were applied to study the adsorption behavior and further understand the adsorption mechanism. Table S6 presented the kinetic parameters. The results predicted by the pseudo-second-order kinetic model closely match those obtained experimentally, and the correlation coefficient (R^2) was also higher than that of the pseudo-first-order model. Accordingly, the pseudo-second-order kinetic model is more suitable for describing the BPA adsorption process, which might also be associated with the strong attraction between the adsorption site and BPA. Lastly, the data were fitted using a Weber-Morris intraparticle diffusion model (Ecer and Şahan 2018) to evaluate BPA diffusion in pores of the adsorbent. Figure 4c and Table S7 show the fitting results and the detailed parameters. There were three steps involved in the adsorption process of BPA onto STPU-AC. In the initial stage of the adsorption process, it was controlled by boundary layer diffusion. Due to its significant specific surface area and porousness, STPU-AC has a high mass transfer capacity, evident from its high K_{d1} . During the second stage, intraparticle diffusion becomes the rate-limiting step. Among the reasons for the decrease in K_{d2} are the reduction in active sites, boundary layer effects, and an increase in mass transfer resistance, which affects diffusion rates in particles. The third stage was adsorption equilibrium. Moreover, the linear fit plot did not go through the origin, showing that rate-controlling steps were not limited to intraparticle diffusion.

Adsorption thermodynamics study

The equilibrium adsorption performance of STPU-AC on BPA was evaluated by adsorption thermodynamic experiments. As depicted in Fig. 4d, STPU-AC has a significantly higher adsorption capacity as BPA concentration increased at a specific temperature until the binding site was saturated. Notably, the uptake capacity of STPU-AC increased with temperature, demonstrating that the removal process

Fig. 5 (a) Co-existed phenol on the adsorption of BPA onto STPU-AC, (b) application in multicomponent solution (100 mg·L⁻¹ BPA, Cu (II) and MB) in the adsorption capacity



of BPA was endothermic. The experimental data was fitted and analyzed with Langmuir and Freundlich adsorption isotherm models with adsorption parameters listed in Table S8. Due to the correlation coefficients (R^2), the Freundlich model was more suitable than the Langmuir model to describe the adsorption process of BPA on STPU-AC, indicating that the adsorption of BPA tends to occur on a non-uniform multilayer surface. Additionally, we applied the Dubinin-Radushkevich (D-R) isotherm (Ceylan et al. 2005) to the adsorption data. Generally, physical adsorption occurs when $E < 8 \text{ kJ}\cdot\text{mol}^{-1}$, ion-exchange process when $8 \leq E \leq 16 \text{ kJ}\cdot\text{mol}^{-1}$, and chemisorption when $E > 16 \text{ kJ}\cdot\text{mol}^{-1}$. BPA had adsorption energies of 0.85,

2.86, and $3.33 \text{ kJ}\cdot\text{mol}^{-1}$ at 25, 35, and 45 °C, respectively (Table S8). Thus, BPA has adsorbed onto STPU-AC through physical adsorption process. A direct comparison of STPU-AC with other adsorbents was difficult due to the different experimental conditions. Notably, the removal of BPA by STPU-AC was more significant than that previously reported for the same type of carbon-based adsorbent (Table S9). This increased adsorption removal rate should be attributed to its large specific surface area, large porosity, and additional adsorption sites. Additionally, STPU-AC was cost-effective and easy to recover, making it a potential adsorbent.

Furthermore, we conducted thermodynamic calculations have been conducted based on the adsorption data

Fig. 6 (a) Desorption efficiency of BPA by various eluents., (b) reusability of STPU-AC in ten adsorption–desorption cycles., (c) N₂ adsorption–desorption isotherms and pore size distribution, and (d) FTIR spectra of pristine and regenerated STPU-AC

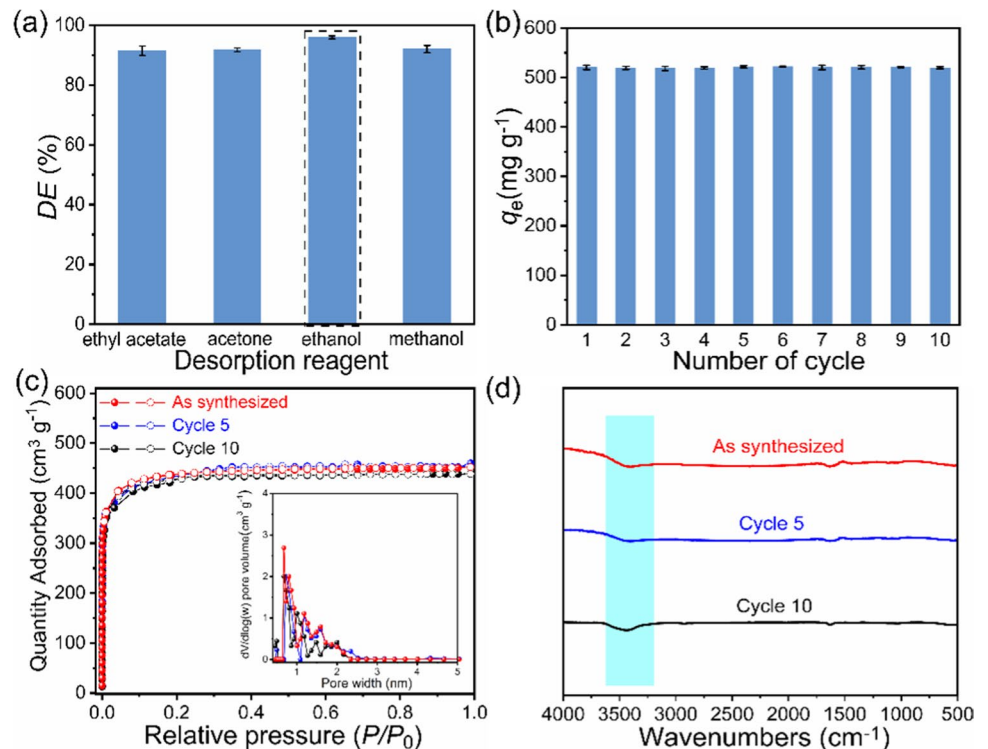
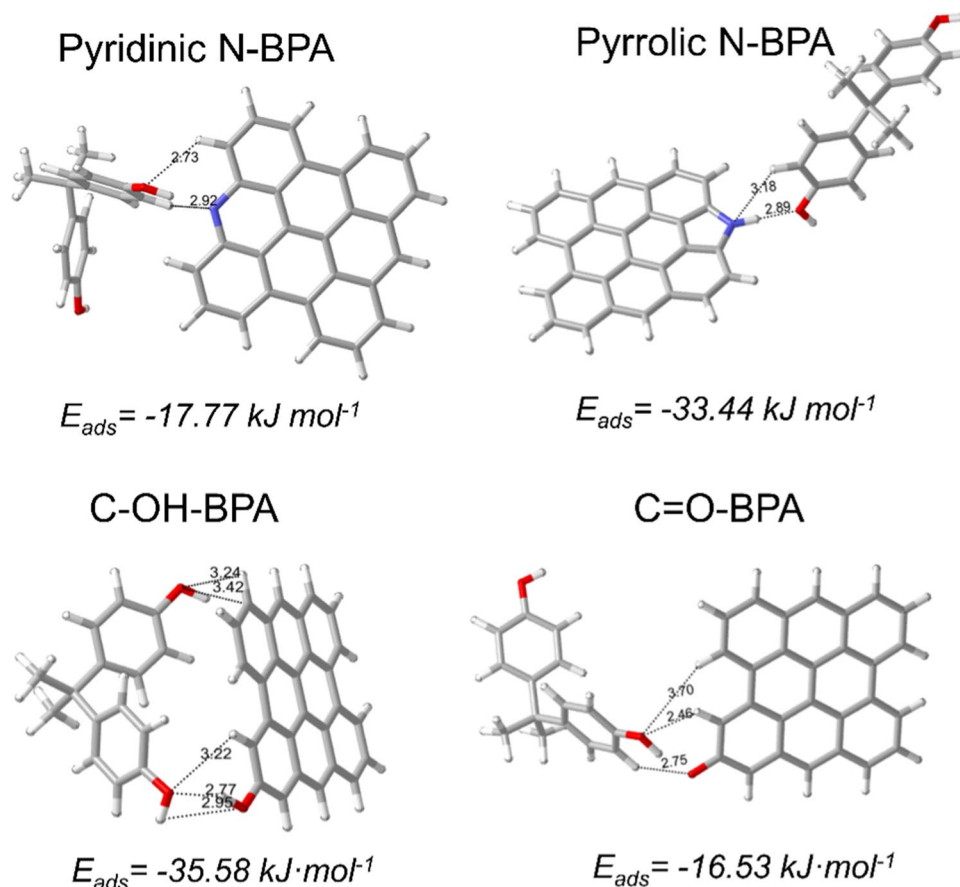


Fig. 7 Optimized configuration and binding energy of CAP molecules on porous carbon, including pyridinic N, pyrrolic N, C–OH, and C=O



at different temperatures. For the three temperatures listed in Table 1, the negative values of ΔG^0 indicated that the adsorption process occurs spontaneously. The absolute value of ΔG^0 increasing with temperature implies that higher temperatures enhance adsorption affinity. The positive ΔH^0 ($65.29 \text{ kJ mol}^{-1}$) indicates that the adsorption process was endothermic, consistent with the isotherm studies. Additionally, the positive values of ΔS^0 ($310.36 \text{ J mol}^{-1} \text{ K}^{-1}$) demonstrates that the adsorption is an entropy-increasing process, revealing the increase of the randomness at the solid–liquid interface. Therefore, the adsorption process of STPU-AC on BPA was a spontaneous endothermic process.

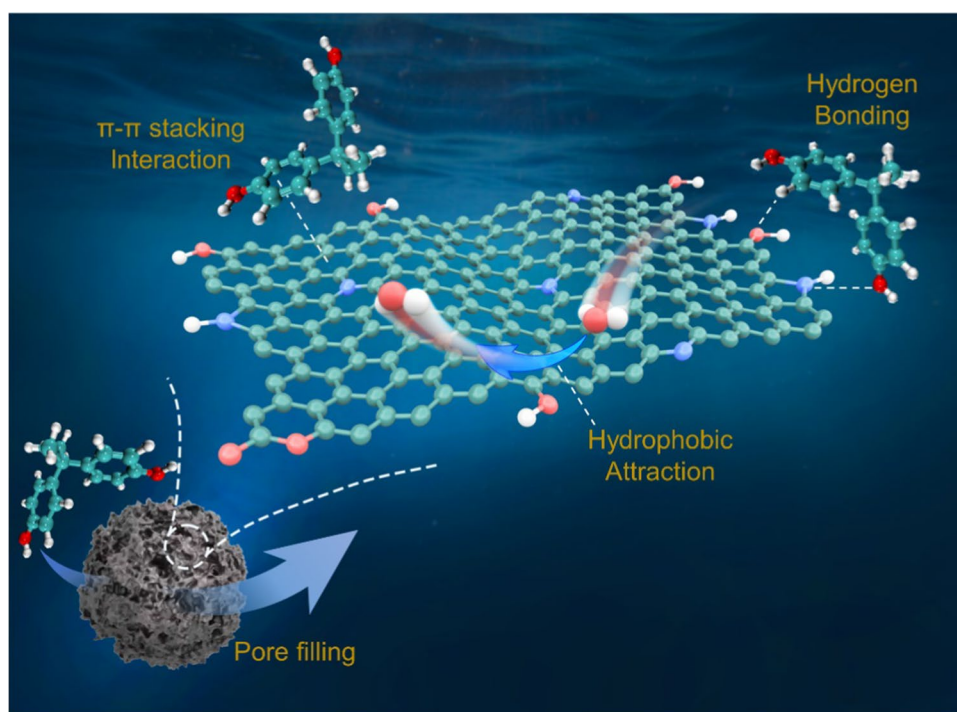
Effects of aqueous solution chemistry on adsorption of BPA

An important parameter that affected adsorption capacity was pH. Here, the uptake of BPA was investigated by STPU-AC at pH values from 2 to 12. As illustrated in Fig. 4e, the adsorption capacity of STPU-AC for BPA remained stable at initial pH values in the 2.0–8.0. As the pH increased to 12, the adsorption capacity of STPU-AC for BPA decreased sharply. The reason for the appearance of the above changes was that most of the BPA in the solution existed in a molecular form when the initial pH was below the pKa value of BPA (9.6–10.4). The formation

of the hydrogen bonding effect between the functional groups on STPU-AC and BPA contributes to the adsorption process (Xiao et al. 2018). Moreover, pH_{PZC} was one of the most crucial parameters in determining the effects of pH on biosorption (Ecer et al. 2020). According to a zeta potential analysis, the pH_{PZC} value of STPU-AC was 5.3. Consequently, the surface charge of the adsorbent was positive at pH < 5.3 and negative at pH > 5.3 (Uzun and Şahan 2017). BPA molecules became ionized in high pH solutions and weakened hydrogen bonds, resulting in electrostatic repulsions and decreased adsorption (Yuan et al. 2022). In the present study, BPA was not ionized at pH 5.0–6.0 in an aqueous solution, indicating that the interaction between STPU-AC and BPA was mainly weak hydrogen bonding, π - π interaction or hydrophobic interaction rather than electrostatic attraction.

Similarly, the ionic strength affects the solubility and hydrophobicity of BPA, subsequently affecting the adsorption properties. Therefore, the effect of ionic strength on the uptake capacity was investigated. The adsorption capacity of STPU-AC for BPA, shown in Fig. 4f, changes slightly as the NaCl concentration increases from 0 to 0.5 mol L^{-1} , most likely due to the BPA solubility decreases as NaCl concentration increases, enhancing the adsorption capacity of STPU-AC for BPA.

Fig. 8 The proposed adsorption mechanism of BPA onto STPU-AC



Performance evaluation of STPU-AC in simulated effluents

Moreover, BPA is an essential derivative of phenol and acetone. The production process of BPA can result in trace amounts of contaminants such as phenol, acetone, and BPA in the wastewater. However, the coexistence of phenolics in the actual aqueous environment can affect their sorption performance. Here, we have investigated the effect of phenol on BPA removal. As shown in Fig. 5a, the adsorption trend of BPA decreased slightly as the phenol concentration increased in the binary-solute system, which may be related to the competition for pore space for physical adsorption.

Additionally, the co-existing contaminants in the wastewater may affect the adsorption of BPA on the sorbent surface in different ways. For example, Meneses et al. (Meneses et al. 2022) observed that the presence of MB and Cr (VI) had no significant effect on the adsorption of BPA. Liu et al. (Liu et al. 2016) investigated the simultaneous adsorption of BPA and Cd^{2+} by activated montmorillonite. They found that when cadmium was present in the solution, the adsorption capacity of BPA was improved. Considering the possible presence of different contaminants (e.g., metal ions, dyes, etc.) in the wastewater, prepared a ternary mixture of BPA, Cu (II), and MB at $100 \text{ mg}\cdot\text{L}^{-1}$ to assess the feasibility of STPU-AC in practical applications. As depicted in Fig. 5b, the co-existing pollutants affected the removal of BPA by STPU-AC due to the competitive

relationship between BPA and Cu (II) and MB. Still, the reduction in adsorption was not significant. Which was consistent with the study by Martín-Lara (Martín-Lara et al. 2020). Overall, STPU-AC has promising applications in the treatment of co-existing wastewater pollutants.

Evaluation of recycling performance

In practical applications, sorbent stability and reusability were essential. Here, the recyclability of STPU-AC was investigated by performing 10 cycles of adsorption/desorption experiments (Text S2). Among the available eluents, ethanol was safe, economical, and exhibited the highest desorption efficiency (Fig. 6a), so it was chosen as the eluent for the subsequent cycle tests. As presented in Fig. 6b, the adsorption capacity of the adsorbent for BPA remained unchanged after ten adsorption cycles. Meanwhile, STPU-AC exhibited similar characteristics before and after adsorption regarding pore structure and functional groups (Fig. 6c and d). These results demonstrate that STPU-AC is a stable adsorbent with excellent regeneration properties.

Adsorption mechanism

First, the interaction of adsorbents was investigated with adsorbed substrates theoretically. The electrostatic potential on the molecular surface (Fig. S2) indicates that the

π electron cloud on the benzene ring was a valid site for adsorption. The structure of BPA contains aromatic units that can provide π -electrons to interact with the sp^2 graphitic carbon in STPU-AC via π – π stacking interactions. Figure 7 and Fig. S3 depicted the optimized geometry and binding energy of bisphenol A at different adsorption sites. It was found that the hydroxyl oxygen and BPA molecules exhibited higher adsorption energies, possibly due to hydrogen bonds between BPA molecules and the functional groups on STPU-AC surfaces, consistent with the XPS results.

Second, STPU-AC possessed a large specific surface area and many microporous structures, which was conducive to the fast adsorption of pollutants, implying a microporous filling effect during the adsorption process. Additionally, the adsorption capacity of BPA was stable over a wide range of pH and ionic strength, suggesting that electrostatic effects rarely affect the adsorption of BPA on STPU-AC. Overall, the adsorption process of BPA on STPU-AC involved multiple interactions, including pore-filling effect, π – π interaction, and hydrogen bonding interaction (Fig. 8).

Conclusions

In this study, STPU-AC is synthesized by a gentle chemically activated two-step pyrolysis method. Due to the unique structure, it significantly facilitated the adsorption of BPA on the active site. According to the batch adsorption results, the adsorption of BPA reached equilibrium within 2 h and followed a pseudo-second-order kinetics model. The Freundlich adsorption isotherms described the adsorption of BPA on a non-uniform multilayer surface. STPU-AC was resistant to acid–base and ionic interference and was desirably reusable. BPA removal was mildly suppressed when STPU-AC was applied to the composite pollutant, demonstrating that the technology can be used for wastewater treatment. Moreover, theoretical calculations further verified the adsorption experiments, where microporous filling, hydrophobic effects, hydrogen bonding, and π – π stacking interactions were associated with the recovery of BPA. Lastly, this study contributed new insights into modifying carbon-based materials and recovering organic pollutants from water.

Supplementary Information The online version contains supplementary material available at <https://doi.org/10.1007/s11356-023-27273-x>.

Author contribution Ke Wang: investigation, writing—original draft, conceptualization, formal analysis, data curation, and validation. Xingzhen Qin: data curation, investigation, and methodology. Kungang Chai: methodology, conceptualization, supervision, writing—review and editing, and formal analysis. Zongwu Wei: conceptualization, supervision, and writing—review and editing. Fan Deng: data curation and investigation. Bingyu Liao: formal analysis and methodology. Jinyu Wu: data

curation and investigation. Zhi Zhang: data curation and investigation. Fang Shen: conceptualization, writing—review and editing, resources, investigation, data curation, funding acquisition, and validation.

Funding This work was supported by the Dean/Opening Project of Guangxi Key Laboratory of Petrochemical Resource Processing and Process Intensification Technology (2021Z009); the Chongzuo Scientific Research and Technology Development Program (20210702).

Data availability The datasets generated during and/or analyzed during the current study are available from the corresponding author on reasonable request.

Declarations

Ethics approval We declare that all ethical guidelines for authors have been followed by all authors.

Consent to participate All authors have given their consent to participate in submitting this manuscript to this journal.

Consent for publication All authors have given their consent to publish this paper in this journal.

Competing interests The authors declare no competing interests.

References

- Ahamad T, Naushad M, Ruksana et al (2019) N/S doped highly porous magnetic carbon aerogel derived from sugarcane bagasse cellulose for the removal of bisphenol-A. *Int J Biol Macromol* 132:1031–1038. <https://doi.org/10.1016/j.ijbiomac.2019.04.004>
- Alves Z, Abreu B, Ferreira NM et al (2021) Enhancing the dispersibility of multiwalled carbon nanotubes within starch-based films by the use of ionic surfactants. *Carbohydr Polym* 273:118531. <https://doi.org/10.1016/j.carbpol.2021.118531>
- Bhatnagar A, Anastopoulos I (2017) Adsorptive removal of bisphenol A (BPA) from aqueous solution: a review. *Chemosphere* 168:885–902. <https://doi.org/10.1016/j.chemosphere.2016.10.121>
- Cazotti JC, Fritz AT, Garcia-Valdez O et al (2020) Graft modification of starch nanoparticles using nitroxide-mediated polymerization and the grafting from approach. *Carbohydr Polym* 228:115384. <https://doi.org/10.1016/j.carbpol.2019.115384>
- Ceylan H, Şahan T, Gürkan R et al (2005) Removal of some heavy metal cations from aqueous solution by adsorption onto natural kaolin. *Adsorpt Sci Technol* 23:519–534. <https://doi.org/10.1260/026361705775212475>
- Chen Z-H, Liu Z, Hu J-Q et al (2020) β -Cyclodextrin-modified graphene oxide membranes with large adsorption capacity and high flux for efficient removal of bisphenol A from water. *J Membr Sci* 595:117510. <https://doi.org/10.1016/j.memsci.2019.117510>
- Cheng J, Gu J-J, Tao W et al (2019) Edible fungus slag derived nitrogen-doped hierarchical porous carbon as a high-performance adsorbent for rapid removal of organic pollutants from water. *Bioresour Technol* 294:122149. <https://doi.org/10.1016/j.biortech.2019.122149>
- Cui Y, Masud A, Aich N et al (2019) Phenol and Cr (VI) removal using materials derived from harmful algal bloom biomass: characterization and performance assessment for a biosorbent, a porous carbon, and Fe/C composites. *J Hazard Mater* 368:477–486. <https://doi.org/10.1016/j.jhazmat.2019.01.075>

- Ecer U, Şahan T (2018) A response surface approach for optimization of Pb (II) biosorption conditions from aqueous environment with *Polyporus squamosus* fungi as a new biosorbent and kinetic, equilibrium and thermodynamic studies. *Desalination Water Treat* 102:229–240. <https://doi.org/10.5004/dwt.2018.21871>
- Ecer Ü, Yılmaz Ş, Şahan T (2020) Investigation of mercury (II) and arsenic (V) adsorption onto sulphur functionalised pumice: a response surface approach for optimisation and modelling. *Int J Environ Anal Chem* 102:7779–7799. <https://doi.org/10.1080/03067319.2020.1838495>
- Ghafari M, Cui Y, Alali A et al (2019) Phenol adsorption and desorption with physically and chemically tailored porous polymers: mechanistic variability associated with hyper-cross-linking and amination. *J Hazard Mater* 361:162–168. <https://doi.org/10.1016/j.jhazmat.2018.08.068>
- Han J, Zhu Z, Li N et al (2021) Metalloporphyrin-based D-A type conjugated organic polymer nanotube for efficient photocatalytic degradation. *Appl Catal B Environ* 291:120108. <https://doi.org/10.1016/j.apcatb.2021.120108>
- Han L, Liu X, Zhang X et al (2022) Preparation of multivariate zirconia metal-organic frameworks for highly efficient adsorption of endocrine disrupting compounds. *J Hazard Mater* 424:127559. <https://doi.org/10.1016/j.jhazmat.2021.127559>
- Heo J, Yoon Y, Lee G et al (2019) Enhanced adsorption of bisphenol A and sulfamethoxazole by a novel magnetic CuZnFe₂O₄-biochar composite. *Biores Technol* 281:179–187. <https://doi.org/10.1016/j.biortech.2019.02.091>
- Humphrey W, Dalke A, Schulten K (1996) VMD: visual molecular dynamics. *J Mol Graph* 14:33–38. [https://doi.org/10.1016/0263-7855\(96\)00018-5](https://doi.org/10.1016/0263-7855(96)00018-5)
- Javed H, Luong DX, Lee C-G et al (2018) Efficient removal of bisphenol-A by ultra-high surface area porous activated carbon derived from asphalt. *Carbon* 140:441–448. <https://doi.org/10.1016/j.carbon.2018.08.038>
- Jiang L, Santiago I, Foord J (2021) A comparative study of fouling-free nanodiamond and nanocarbon electrochemical sensors for sensitive bisphenol A detection. *Carbon* 174:390–395. <https://doi.org/10.1016/j.carbon.2020.11.073>
- Karthikeyan BS, Ravichandran J, Mohanraj K et al (2019) A curated knowledgebase on endocrine disrupting chemicals and their biological systems-level perturbations. *Sci Total Environ* 692:281–296. <https://doi.org/10.1016/j.scitotenv.2019.07.225>
- Khan NA, Hasan Z, Jhung SH (2013) Adsorptive removal of hazardous materials using metal-organic frameworks (MOFs): a review. *J Hazard Mater* 244–245:444–456. <https://doi.org/10.1016/j.jhazmat.2012.11.011>
- Kim B, Jang J, Lee DS (2022) Enhanced photocatalytic degradation of bisphenol A by magnetically separable bismuth oxyiodide magnetite nanocomposites under solar light irradiation. *Chemosphere* 289:133040. <https://doi.org/10.1016/j.chemosphere.2021.133040>
- Kittappa S, Jang M, Ramalingam M et al (2020) Amine functionalized magnetic nano-composite materials for the removal of selected endocrine disrupting compounds and its mechanism study. *J Environ Chem Eng* 8:103839. <https://doi.org/10.1016/j.jece.2020.103839>
- Lee MY, Ahmed I, Yu K et al (2021) Aqueous adsorption of bisphenol A over a porphyrinic porous organic polymer. *Chemosphere* 265:129161. <https://doi.org/10.1016/j.chemosphere.2020.129161>
- Liu C, Wu P, Zhu Y et al (2016) Simultaneous adsorption of Cd²⁺ and BPA on amphoteric surfactant activated montmorillonite. *Chemosphere* 144:1026–1032. <https://doi.org/10.1016/j.chemosphere.2015.09.063>
- Lu T, Chen F (2012) Multiwfn: A multifunctional wavefunction analyzer. *J Comput Chem* 33:580–592. <https://doi.org/10.1002/jcc.22885>
- Lv Y, Ma J, Liu K et al (2021) Rapid elimination of trace bisphenol pollutants with porous β -cyclodextrin modified cellulose nanofibrous membrane in water: adsorption behavior and mechanism. *J Hazard Mater* 403:123666. <https://doi.org/10.1016/j.jhazmat.2020.123666>
- M'Rabet C, Kéfi-Daly Yahia O, Couet D et al (2019) Consequences of a contaminant mixture of bisphenol A (BPA) and di-(2-ethylhexyl) phthalate (DEHP), two plastic-derived chemicals, on the diversity of coastal phytoplankton. *Mar Pollut Bull* 138:385–396. <https://doi.org/10.1016/j.marpolbul.2018.11.035>
- Martinez R, Navarro-Martin L, van Antrop M et al (2020) Changes in lipid profiles induced by bisphenol A (BPA) in zebrafish elutheroembryos during the yolk sac absorption stage. *Chemosphere* 246:125704. <https://doi.org/10.1016/j.chemosphere.2019.125704>
- Martín-Lara MA, Calero M, Ronda A et al (2020) Adsorptive behavior of an activated carbon for bisphenol A removal in single and binary (bisphenol A-heavy metal) solutions. *Water* 12. <https://doi.org/10.3390/w12082150>
- Meneses IP, Novaes SD, Dezotti RS et al (2022) CTAB-modified carboxymethyl cellulose/bagasse cryogels for the efficient removal of bisphenol A, methylene blue and Cr (VI) ions: batch and column adsorption studies. *J Hazard Mater* 421:126804. <https://doi.org/10.1016/j.jhazmat.2021.126804>
- Mpatani FM, Aryee AA, Kani AN et al (2020) Uptake of micropollutant-bisphenol A, methylene blue and neutral red onto a novel bagasse- β -cyclodextrin polymer by adsorption process. *Chemosphere* 259:127439. <https://doi.org/10.1016/j.chemosphere.2020.127439>
- Mpatani FM, Han R, Aryee AA et al (2021) Adsorption performance of modified agricultural waste materials for removal of emerging micro-contaminant bisphenol A: a comprehensive review. *Sci Total Environ* 780:146629. <https://doi.org/10.1016/j.scitotenv.2021.146629>
- Pan B, Lin D, Mashayekhi H et al (2008) Adsorption and hysteresis of bisphenol A and 17 α -ethinyl estradiol on carbon nanomaterials. *Environ Sci Technol* 42:5480–5485. <https://doi.org/10.1021/es8001184>
- Pellicer-Castell E, Belenguer-Sapiña C, Amorós P et al (2022) A β -cyclodextrin sorbent based on hierarchical mesoporous silica for the determination of endocrine-disrupting chemicals in urine samples. *J Chromatogr A* 1671:463007. <https://doi.org/10.1016/j.chroma.2022.463007>
- Qu J, Zhang X, Liu S et al (2022) One-step preparation of Fe/N co-doped porous biochar for chromium (VI) and bisphenol A decontamination in water: insights to co-activation and adsorption mechanisms. *Bioresource Technol* 361:127718. <https://doi.org/10.1016/j.biortech.2022.127718>
- Rana D, Narbaitz RM, Garand-Sheridan A-M et al (2014) Development of novel charged surface modifying macromolecule blended PES membranes to remove EDCs and PPCPs from drinking water sources. *J Mater Chem A* 2:10059–10072. <https://doi.org/10.1039/c4ta01530d>
- Ruiz E (2008) Exchange coupling constants using density functional theory: the MOX suite. *Chem Phys Lett* 460:336–338. <https://doi.org/10.1016/j.cplett.2008.05.073>
- Shao P, Pei J, Tang H et al (2021) Defect-rich porous carbon with anti-interference capability for adsorption of bisphenol A via long-range hydrophobic interaction synergized with short-range dispersion force. *J Hazard Mater* 403:123705. <https://doi.org/10.1016/j.jhazmat.2020.123705>
- Uzun Y, Şahan T (2017) Optimization with response surface methodology of biosorption conditions of Hg (II) ions from aqueous media by *polyporus squamosus* fungi as a new biosorbent. *Arch Environ Prot* 43:37–43. <https://doi.org/10.1515/aep-2017-0015>
- Wang T, Xue L, Zheng L et al (2021a) Biomass-derived N/S dual-doped hierarchically porous carbon material as effective adsorbent

- for the removal of bisphenol F and bisphenol S. *J Hazard Mater* 416:126126. <https://doi.org/10.1016/j.jhazmat.2021.126126>
- Wang Y, Wei X, Qi Y et al (2021b) Efficient removal of bisphenol-A from water and wastewater by Fe₂O₃-modified graphene oxide. *Chemosphere* 263:127563. <https://doi.org/10.1016/j.chemosphere.2020.127563>
- Wang T, Zhang H, Liu Y et al (2022) Ultrathin porous carbon nanosheet as an efficient adsorbent for the removal of bisphenol A: the overlooked role of topological defects. *Chemosphere* 306:135549. <https://doi.org/10.1016/j.chemosphere.2022.135549>
- Wei D, Zhao C, Khan A et al (2019) Sorption mechanism and dynamic behavior of graphene oxide as an effective adsorbent for the removal of chlorophenol based environmental-hormones: a DFT and MD simulation study. *Chem Eng J* 375:121964. <https://doi.org/10.1016/j.cej.2019.121964>
- Xiao X, Zhang F, Feng Z et al (2015) Adsorptive removal and kinetics of methylene blue from aqueous solution using NiO/MCM-41 composite. *Physica E Low Dimens Syst Nanostruct* 65:4–12. <https://doi.org/10.1016/j.physe.2014.08.006>
- Xiao P, Wang P, Li H et al (2018) New insights into bisphenols removal by nitrogen-rich nanocarbons: synergistic effect between adsorption and oxidative degradation. *J Hazard Mater* 345:123–130. <https://doi.org/10.1016/j.jhazmat.2017.11.001>
- Xu G, Xie X, Qin L et al (2019) Simple synthesis of a swellable porous β -cyclodextrin-based polymer in the aqueous phase for the rapid removal of organic micro-pollutants from water. *Green Chem* 21:6062–6072. <https://doi.org/10.1039/c9gc02422k>
- Yang C, Wang P, Li J et al (2021) Photocatalytic PVDF ultrafiltration membrane blended with visible-light responsive Fe (III)-TiO₂ catalyst: degradation kinetics, catalytic performance and reusability. *Chem Eng J* 417:129340. <https://doi.org/10.1016/j.cej.2021.129340>
- Yao X, Zhou J, Liu Z (2022) Study on adsorption of low-concentration methyl mercaptan by starch-based activated carbon. *Chemosphere* 302:134901. <https://doi.org/10.1016/j.chemosphere.2022.134901>
- Yuan W, Zhou L, Zhang Z et al (2022) Synergistic dual-functionalities of starch-grafted-styrene hydrophilic porous resin for efficiently removing bisphenols from wastewater. *Chem Eng J* 429:132350. <https://doi.org/10.1016/j.cej.2021.132350>
- Zhang Y, Wang F, Ou P et al (2018) High efficiency and rapid degradation of bisphenol A by the synergy between adsorption and oxidization on the MnO₂@nano hollow carbon sphere. *J Hazard Mater* 360:223–232. <https://doi.org/10.1016/j.jhazmat.2018.08.003>
- Zhang B, Jin Y, Huang X et al (2022a) Biological self-assembled hyphae/starch porous carbon composites for removal of organic pollutants from water. *Chem Eng J* 450:138264. <https://doi.org/10.1016/j.cej.2022.138264>
- Zhang Y, Chen Y, Lei Y et al (2022b) Tailoring diameters of carbon nanofibers with optimal mesopores to remarkably promote hemin adsorption toward ultrasensitive detection of bisphenol A. *Food Chem* 383:132628. <https://doi.org/10.1016/j.foodchem.2022.132628>
- Zhao L, Zhang X, Liu Z et al (2021) Carbon nanotube-based electrocatalytic filtration membrane for continuous degradation of flow-through bisphenol A. *Sep Purif Technol* 265:118503. <https://doi.org/10.1016/j.seppur.2021.118503>
- Zhao Z, Liu Y, Zhang Y et al (2022) Fabricating hypercrosslinked aromatic-rich starch urethane polymer with enhanced adsorption performance for separation of acetophenone and 1-phenylethanol. *React Funct Polym* 175:105272. <https://doi.org/10.1016/j.reactfunctpolym.2022.105272>
- Zhou L, Liang Q, Chai K et al (2020) A cost-effective β -cyclodextrin polymer for selective adsorption and separation of acetophenone and 1-phenylethanol via specific noncovalent molecular interactions. *React Funct Polym* 146:104448. <https://doi.org/10.1016/j.reactfunctpolym.2019.104448>

Publisher's note Springer Nature remains neutral with regard to jurisdictional claims in published maps and institutional affiliations.

Springer Nature or its licensor (e.g. a society or other partner) holds exclusive rights to this article under a publishing agreement with the author(s) or other rightsholder(s); author self-archiving of the accepted manuscript version of this article is solely governed by the terms of such publishing agreement and applicable law.